catalysts

MDPI

Article

Sustainable Solar Light Photodegradation of Diclofenac by Nano- and Micro-Sized $SrTiO_3$

Melissa G. Galloni [1,2], Giuseppina Cerrato [2,3], Alessia Giordana [2,3], Ermelinda Falletta [1,2,*] and Claudia L. Bianchi [1,2]

[1] Dipartimento di Chimica, Università degli Studi di Milano, Via Camillo Golgi 19, 20133 Milano, Italy; melissa.galloni@unimi.it (M.G.G.); claudia.bianchi@unimi.it (C.L.B.)
[2] Consorzio Interuniversitario Nazionale per la Scienza e Tecnologia dei Materiali (INSTM), Via Giusti 9, 50121 Florence, Italy; giuseppina.cerrato@unito.it (G.C.); alessia.giordana@unito.it (A.G.)
[3] Dipartimento di Chimica, Università degli Studi di Torino, Via Pietro Giuria 7, 10125 Torino, Italy
* Correspondence: ermelinda.falletta@unimi.it; Tel.: +39-02-503114410

Abstract: Currently, photocatalytic reactions under solar illumination have attracted worldwide attention due to the tremendous set of associated environmental problems. Taking sunlight into account, it is indispensable to develop highly effective photocatalysts. Strontium titanate, $SrTiO_3$ (STO), is a cubic perovskite-type semiconductor, an inexpensive material with high thermal stability and corrosion resistance that exhibits a similar energy bandgap to TiO_2 and can represent an interesting alternative in photocatalytic applications. Particle size can significantly affect both photocatalytic and photoelectrochemical properties of a photocatalyst, thus altering the photooxidation of organic pollutants in air or water. In this context, this research aims at investigating the photocatalytic features of nano- and micro-sized commercial STO powders towards the photodegradation of diclofenac (DFC), a non-steroidal, anti-inflammatory drug, widely used as analgesic, antiarthritic, and antirheumatic. Both nano- and micro-STO photocatalysts exhibited remarkable photocatalytic efficiency towards DCF, reaching photodegradation efficiency higher than 90% within one hour. Results obtained in simulated drinking water were also compared to those obtained in ultrapure water. Both STOs showed good stability during recycling tests, maintaining high performances after three cycles. Eventually, active species were identified using various scavengers by trapping holes and radicals generated during the photocatalytic degradation process.

Keywords: water remediation; diclofenac; strontium titanate; solar photodegradation

Citation: Galloni, M.G.; Cerrato, G.; Giordana, A.; Falletta, E.; Bianchi, C.L. Sustainable Solar Light Photodegradation of Diclofenac by Nano- and Micro-Sized $SrTiO_3$. *Catalysts* **2022**, *12*, 804. https://doi.org/10.3390/catal12080804

Academic Editors: Detlef W. Bahnemann, Ewa Kowalska, Ioannis Konstantinou, Magdalena Janus, Vincenzo Vaiano, Wonyong Choi and Zhi Jiang

Received: 1 July 2022
Accepted: 20 July 2022
Published: 22 July 2022

1. Introduction

In the last decades, rapid industrialization and urbanization have raised the demand for new technologies for water decontamination to improve the health standards of world population [1–4]. In this context, it has been demonstrated that the main source of water pollution comes from sewage discharge and contaminated effluents in watercourses. Recent statistics report that lack of proper sanitation forces 2.4 billion people daily to use unsafe sources of water, experiencing diseases such as hepatitis, dysentery, and cholera, which in the worst cases can lead to cancer or death [5,6].

Traditionally, several treatment methods have been used to purify water, such as sedimentation, filtration, adsorption, biological digestion, and chemical disinfection, but, unfortunately, they could be insufficient in the removal of persistent pollutants [2,7–10]. For these reasons, researchers are looking for economic and smart techniques able to uniformly eliminate all the dangerous molecules located in water matrices. Among all the possible approaches, advance oxidation processes (AOPs), such as heterogeneous photocatalysis, offer green and simple solutions to oxidize organic compounds to CO_2 [11–14]. In this field, the most studied photocatalyst is titanium dioxide (TiO_2), a semiconductor extremely active under UV light in producing oxidative hydroxyl radicals (OH) [15–20]. Despite

this, bare TiO_2 has shown poor efficiency in the visible range of light radiation, and it has been recently recognized as a potentially carcinogenic material when used in nanometric form [21,22]. In view of overcoming these issues, TiO_2 doping with metal or non-metal species (e.g., Cu, Co, Ag, Eu, Mo, W) has been proposed as an effective method to improve its overall characteristics, in particular for the exploitation of solar radiation as an energy source [23–29]. Moreover, alternative materials are being explored. Among these, strontium titanate, $SrTiO_3$ (STO), has demonstrated optimum features to be applied as a photocatalyst for the removal of organic pollutants [30–35]. In fact, its typical perovskite-type phase and its chemical and physical stability are advantages for strong catalytic activity [36]. To boost its performance, in many studies, metals have been additionally introduced to dope its perovskite structure, in particular to improve its efficiency under visible light radiation [37–41].

Several classes of pollutants are present in contaminated water matrices: fertilizers, herbicides, and insecticides, mainly deriving from agricultural industry, as well as pharmaceuticals [42–47]. These latter are continuously increasing in the aquatic environment because they are not completely removed when passing through plants devoted to the wastewater treatment [48]. Among them, diclofenac (DCF) is a synthetic non-steroidal anti-inflammatory drug, mainly used as analgesic, antiarthritic, and antirheumatic, but also in outpatient care. Its world consumption consists of about 940 tons *per* year, considering 100 mg as the daily dose [49–52]. DCF enters the aquatic environment by direct disposal from households, human and animal excretion, and medical care, and it is characterized by high stability [53]. Following these premises, apprehension towards DCF has been enhanced because of its long-term resistance and bioaccumulation [54,55]. In fact, it is already found in drinking water reservoirs, and for its bioavailability and poor biodegradability in aquatic biota, it was reported by the European Union, Directive 2013/39/EU(2013), as a priority hazardous substance [12,55–57].

Based on these considerations, researchers have aimed their efforts at improving technologies for its degradation, but so far, application of the studied materials in real contaminated water remains a challenge [12,17,18]. In real matrices, the presence of competitive compounds could limit the catalyst's efficiency. In particular, the presence of inorganic species, such as salts and metals, could deactivate the photocatalyst, decreasing the efficacy of the AOP processes [58,59]. Moreover, focusing the attention on the photocatalytic properties of the targeted photocatalyst, it is also known that the particle size (nano- or micro-metric) can be a key parameter in altering the photooxidation of organic pollutants in air or water.

In this work, for the first time, the photodegradation efficiency of two STOs (micro- and nano-sized, respectively) was comparatively investigated towards DCF abatement under solar light irradiation. Tests were carried out by dissolving DCF in two different matrices (ultrapure water, UW, and simulated drinking water, DW) to evaluate the potential application of the selected photocatalysts in a real environment. The reusability of STOs has been adequately investigated, showing high stability for up to three runs. Eventually, active species were identified using various scavengers by trapping holes and radicals generated during the photocatalytic degradation process.

2. Results and Discussion

2.1. Photocatalyst Characterization

Two commercial strontium titanates (labelled as STOm and STOn, i.e., micro- and nano-sized, respectively) were properly characterized according to a combination of physico-chemical techniques, whose results are described below.

X-ray powder diffraction (XRPD) patterns of samples (Figure 1) exhibit good crystallinity.

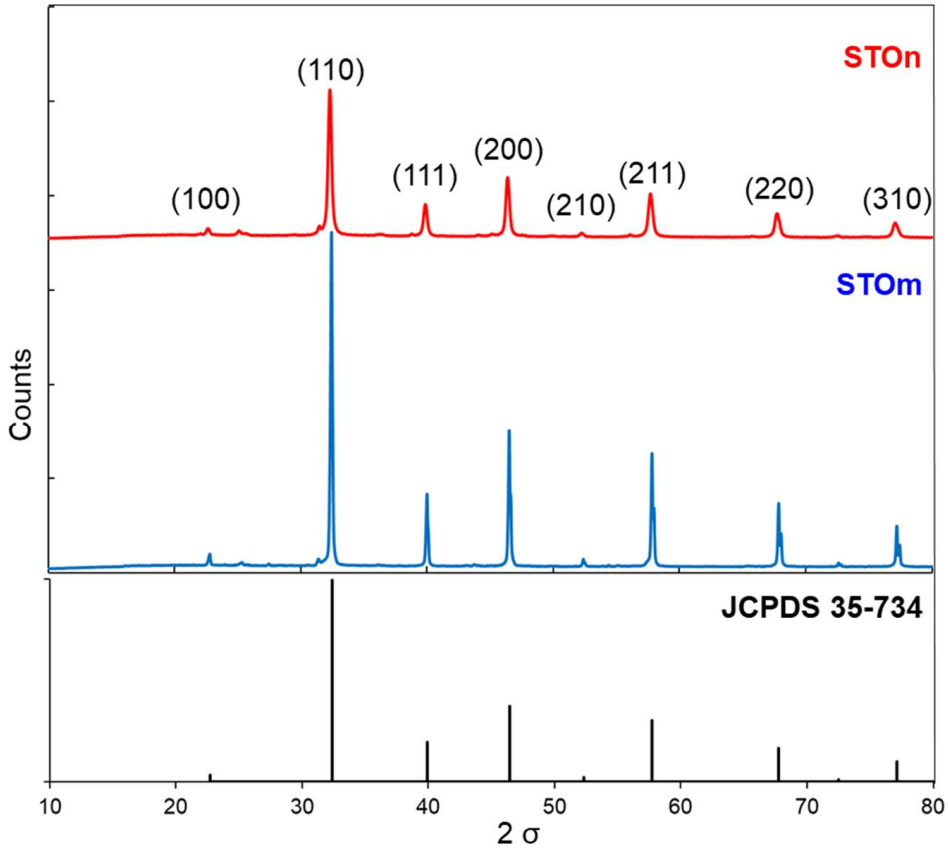

Figure 1. XRPD patterns of STOn and STOm (red and blue lines, respectively).

As shown in Figure 1, their diffraction patterns fit to peak positions of the standard cubic perovskite structure (space group: Pm3m) of STO (JCPDS n. 35-734), whereas the other peaks can be attributed to traces of $SrCO_3$ (JCPDS 05-0418). Moreover, as expected, if compared to those of STOm, the diffraction peaks of STOn show weakened intensity which, coupled to the peak broadening, suggest smaller particle size, as furtherly confirmed by Scherrer equation: 98.3 nm and 30.5 nm for STOm and STOn, respectively.

N_2 adsorption/desorption isotherms collected at −196 °C (Figure 2) are of Type IV, according to the IUPAC classification [60,61].

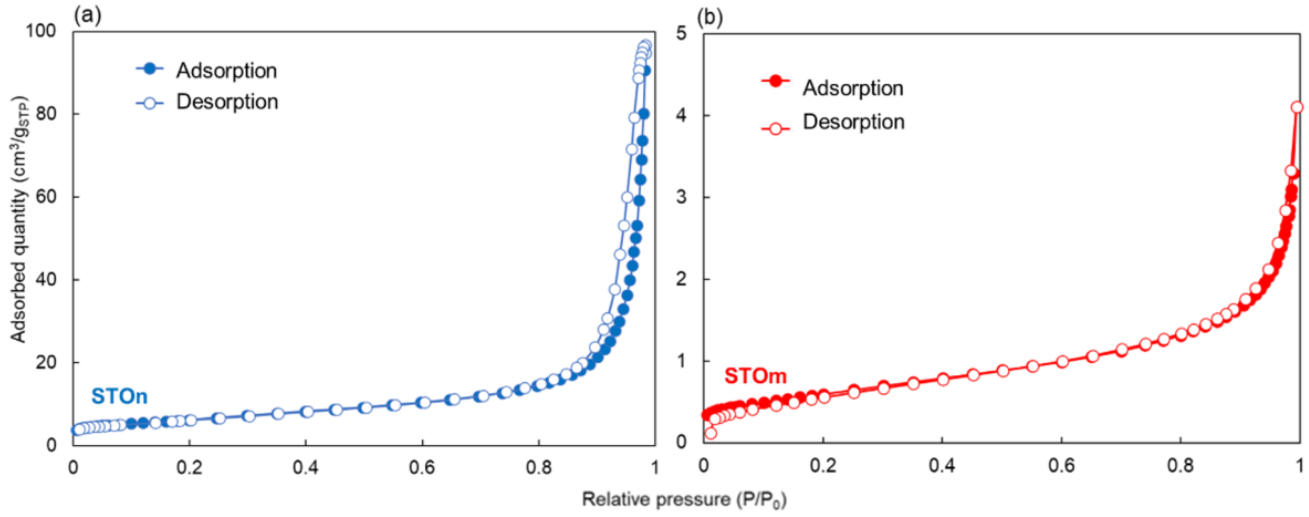

Figure 2. N_2 adsorption/desorption isotherms at −196 °C for STOn (**a**) and STOm (**b**).

They possess a hysteresis zone (H3 type, de Boer's classification), typical of mesoporous materials, and only minor microporosity [62,63]. In particular, STOm is characterized by a lower value of specific surface area than STOn (respectively, 2 vs. 21 $m^2 \cdot g^{-1}$), in accordance with XRPD results.

Surface properties (i.e., chemical composition and state of the main species present over sample surfaces) were investigated by X-ray photoelectron spectroscopy (XPS).

The obtained results are summarized in Table S1 and Figure 3, Figure 4 and Figure S1, in terms of surface concentrations (in atomic percent), survey spectra, and high resolution (HR) spectra of Sr, Ti, and O for STOn and STOm, respectively.

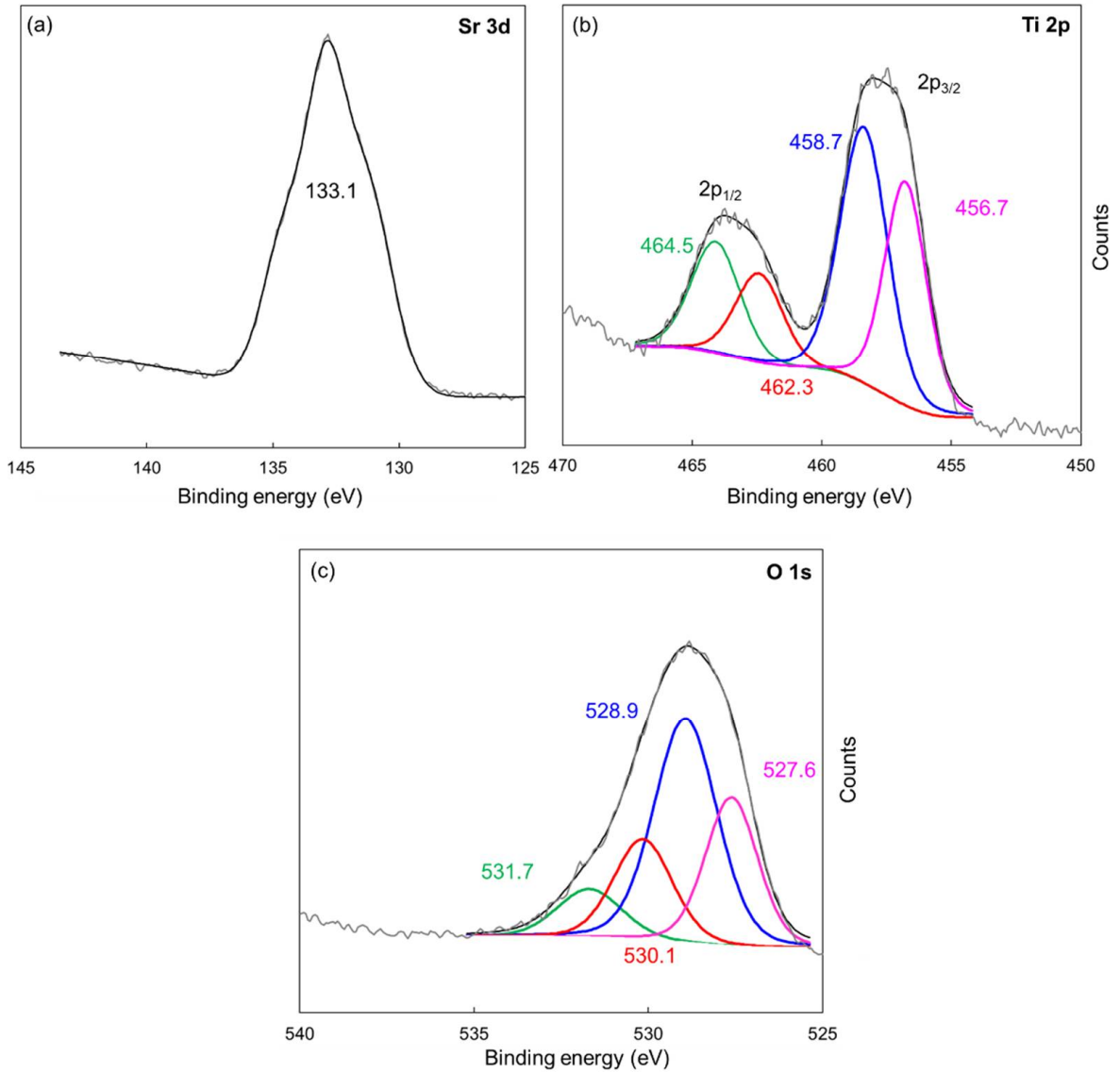

Figure 3. XPS HR spectra of Sr 3d, Ti 2p, and O 1s of STOn.

In general, as expected, both survey spectra (Figure S1) confirm the presence of Sr, Ti, O, and C at the photocatalyst surfaces. In any case, the presence of carbon besides the adventitious one could be ascribed to carbonate species on surfaces (Figure S2), according to XRPD analyses (Figure 1) [64].

Concerning the core energy levels (i.e., Sr 3d, Ti 2p, and O 1s, Figures 3 and 4 for STOn and STOm, respectively), both samples show very similar results. Sr $3d^{5/2}$ core level centered at 133.1 eV in the STOn spectrum (Figure 3a) corresponds to +2 valence of Sr [65,66].

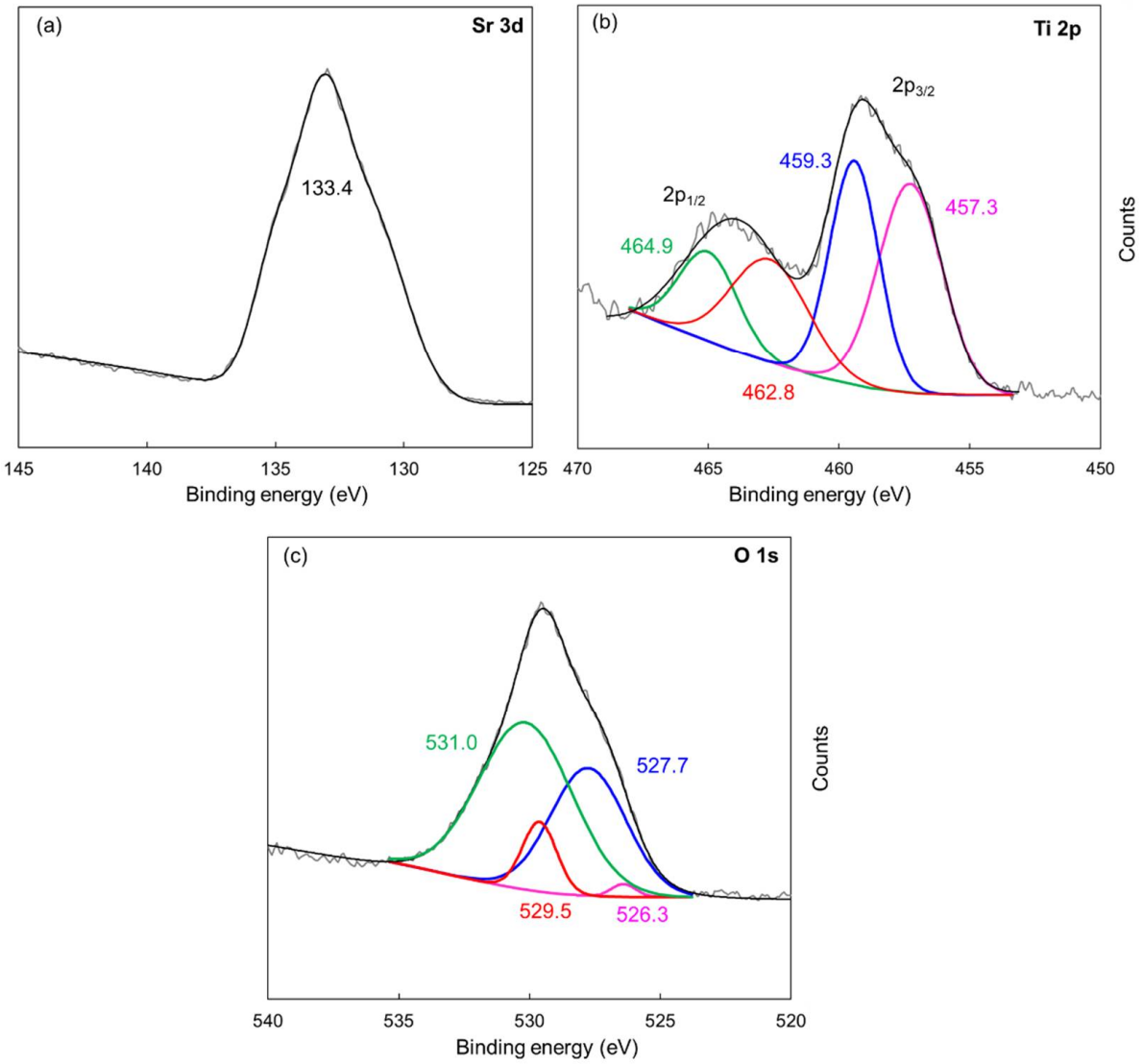

Figure 4. XPS HR spectra of Sr 3d, Ti 2p, and O 1s of STOm.

Regarding the Ti 2p signals, the doublet at 458.7 and 464.5 eV can be assigned to Ti 2p 3/2 and $\frac{1}{2}$ components of Ti^{4+}. The second doublet at 456.7 and 462.3 eV is related to the presence of Ti^{3+} species in the material (Figure 3b) [67].

Eventually, the O 1s spectrum (Figure 3c) shows a complex peak structure. The fitted two peaks located at binding energies of 527.8 and 528.9 eV are assigned to the lattice oxygen ion and oxygen vacancy, whereas the last two at 530.1 and 531.7 eV are related to the adsorption of OH species on the STO surface [68]. Similar results were obtained for STOn (Figure 4c).

Bandgap evaluation was carried out from UV–Vis diffuse reflectance spectra (UV–DRS) collected in the 200–800 nm interval (Figure 5).

Both samples present higher absorbance at wavelengths shorter than 400 nm, resulting from electron transitions of valence band to conduction band, and the values of absorbance decrease as the photon energy is lower than the bandgap energy of each material.

As expected, the optical absorption of nano-sized oxide (STOn) is much stronger than that of the micrometric material (Figure 5a), in agreement with Liu and Reinosa et al. for TiO_2-based materials [69,70]. In particular, this behavior has been detected in 230 nm < λ < 330 nm. The resulting values equal to about 3.23 and 3.24 eV for STOm and STOn, respectively, implying that the photocatalytic properties might exist under solar light irradiation, exploiting the UV component. Moreover, according to previous

studies [69,70], the differences found between the two bandgap values could be ascribed to the particles' size, impacting on the crystalline structure and defects of the STO samples, also in agreement to XRPD results.

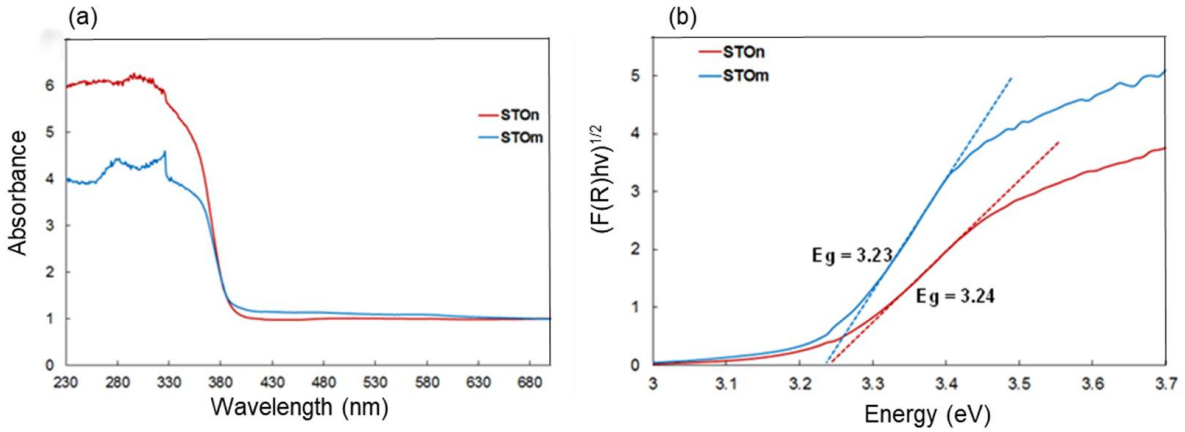

Figure 5. UV–visible absorption spectra (**a**) and Tauc plots (**b**) for STOm (blue line) and STOn (red line).

To obtain some information about the functionalities eventually present at the surface of both STO materials, Fourier transform infrared (FT-IR) spectroscopy has been employed; results are depicted in Figure 6.

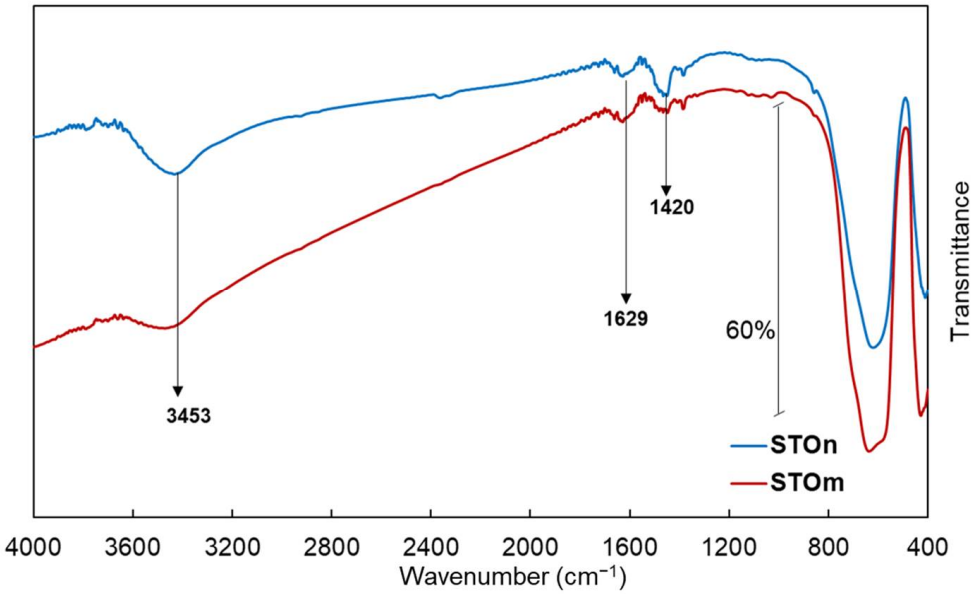

Figure 6. FT-IR spectra of STOm (red line) and STOn (blue line).

The broad absorption located at $\nu > 3000$ cm^{-1} is assigned to the stretching vibration of all the OH groups present on both STOs, including those deriving from undissociated water molecules present at the surface, whose spectroscopic counterpart (δ_{HOH}, bending mode) is included in the envelope right above 1600 cm^{-1} [65]. Eventually, the complex absorption bands (including the 1629 cm^{-1} component just discussed) located in the 1700–1300 cm^{-1} range can be related to some spectral modes due to traces of carbonate species still present as residues of the synthetic procedure [71]. Bands below 1000 cm^{-1} can be related to some $SrTiO_3$ crystal lattice vibrations [72].

Sample morphology was investigated by conventional transmission and scanning electron microscopies (C-TEM and SEM). Micrographs of STOn (Figure 7a,b) show almost cube-shaped particles, exhibiting an average dimension of about 40 nm. In contrast, STOm

particles (Figure 7c,d) are much larger, characterized by either smooth edges or slightly sharper contours, with irregular dimension spanning the range of 200 nm–1.5 μm.

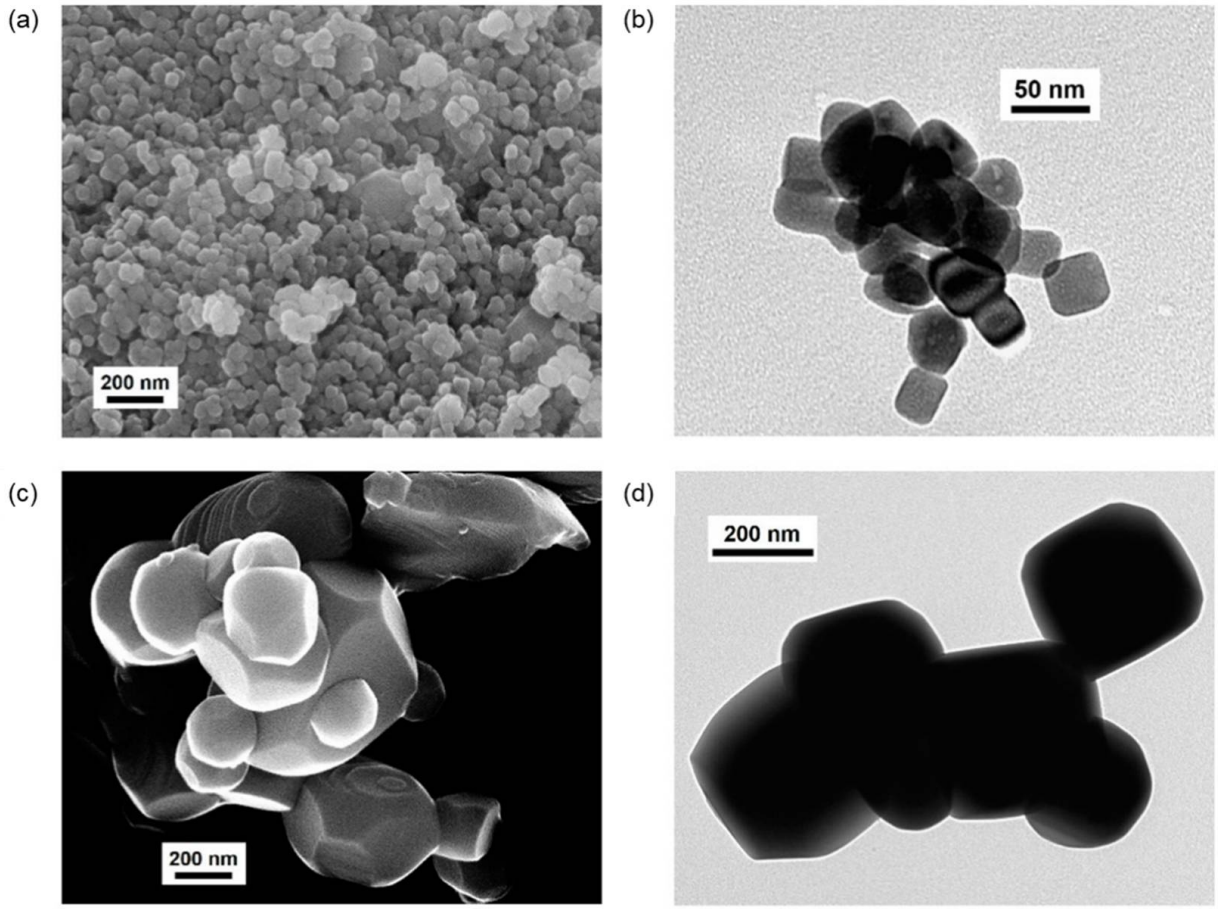

Figure 7. SEM and TEM images of STOn (**a**,**b**) and STOm (**c**,**d**).

In the Electronic Supplementary Material (ESI), the determination of isoelectric point (IEP) is provided (Paragraph S1 and Figure S3).

2.2. Diclofenac Abatement

Both samples were tested for DCF photodegradation under solar light irradiation.

Before starting the photocatalytic investigation, a photolysis test was performed in ultrapure water (UW) and in the absence of any photocatalysts. Results indicate that photolysis has a negligible effect on the DCF degradation (Figure S4).

The photocatalytic activity of samples was studied under different conditions to investigate the effect of some key parameters, such as photocatalyst dose and type of water matrix (ultrapure water, UW, and simulated drinking water, DW).

It is known that photocatalysis is a catalyst-mass-dependent reaction [73]. However, although large quantities of active species (hydroxyl radicals and/or electrons by absorbing more photons) correspond to large quantities of catalyst, a photocatalyst excess could increase the solution turbidity, reducing the energy absorption from light radiation, thereby decreasing the degradation efficiency. Moreover, proper doses of photocatalyst in the photodegradation system can reduce costs from an economic viewpoint. Therefore, at first, the effect of photocatalyst dose towards DCF photodegradation in ultrapure water (UW) under solar light irradiation was properly investigated. The main results are reported in Figure 8.

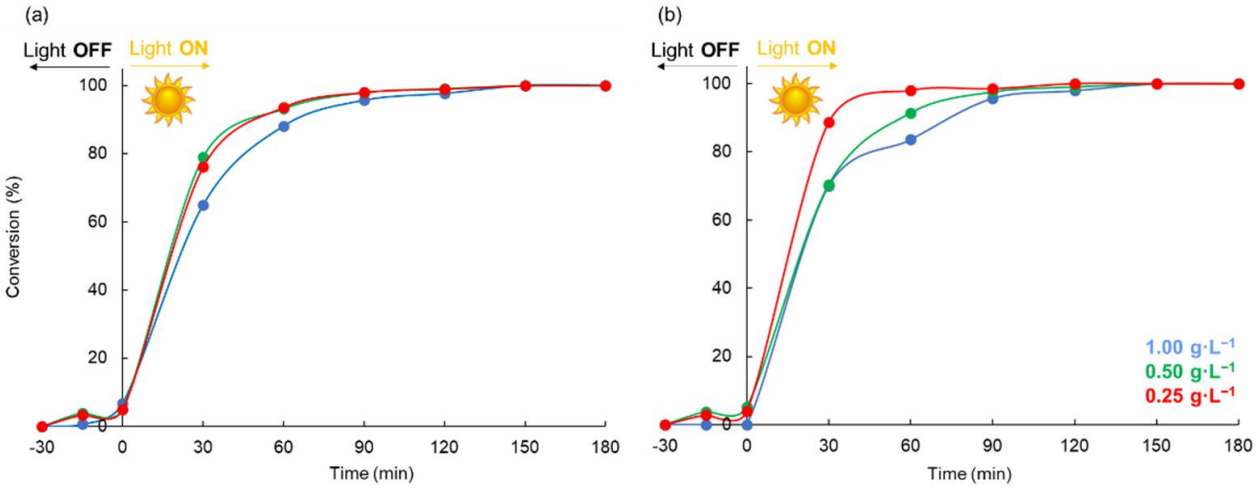

Figure 8. Effect of photocatalyst dose on DCF photodegradation in UW ((**a**) STOn; (**b**) STOm).

Dark adsorption tests led to a negligible DCF loss for both samples. In contrast, both oxides exhibit extraordinarily high activity. In general, the degradation efficiency increased as the dose decreased from 1.00 to 0.25 g·L^{-1}. In fact, as reported above, an excess of photocatalyst dose can increase the solution turbidity and simultaneously reduce the light penetration into the reaction system. Consequently, the lower light absorption of the photocatalyst decreases the degradation efficiency. This effect is much more pronounced for STOm than for the corresponding nanometric material. Nanoparticles' size is a crucial factor for their use in several fields. In particular, for photocatalytic applications, large particles or their aggregates can affect the optical properties of the solution by strong scattering and/or absorption of rays [74]. As shown in Figure 8, STOm is able to degrade 98% of the DCF within one hour when the catalyst concentration is 0.25 g·L^{-1}. This percentage decreases to 91% when the photocatalyst concentration is increased up to 0.50 g·L^{-1} and reaches 85% if the photocatalyst dose is doubled again. Conversely, the effect of photocatalyst dose is less marked for nanometric STO. In fact, both tests carried out using the concentration of 0.50 g·L^{-1} and 0.25 g·L^{-1} of STOn lead to 94% DCF degradation in one hour. However, even in this case, a further increase of photocatalyst amount causes a decrease in the efficiency of the catalytic system (up to 88%).

Figure 9 suggests that DCF photodegradation carried out by both STOs follows second-order kinetics, according to the following equation:

$$\frac{t}{q \cdot t} = \frac{t}{k_2 \cdot q_e^2} + \frac{t}{q_e} \quad (1)$$

where q_e and q are the amounts of photodegraded DCF by STO at the equilibrium and time t, respectively (mg·g^{-1}), whereas k_2 is the rate constant of pseudo second-order kinetics (min^{-1}).

From the slope and the intercept of the graphics (t/qt vs. t, Figure 9) pseudo second-order rate constants were calculated (k_2), and they the results were 0.016 and 0.006 min^{-1} for STOn and STOm, respectively.

This model predicts that *intra*-particle diffusion/transport process is the rate determining step that may involve valence forces through sharing or exchange of electrons between the pollutant and photoreactive species.

Total organic carbon (TOC) measurements showed that STO do not exhibit high mineralization ability (Figure S5).

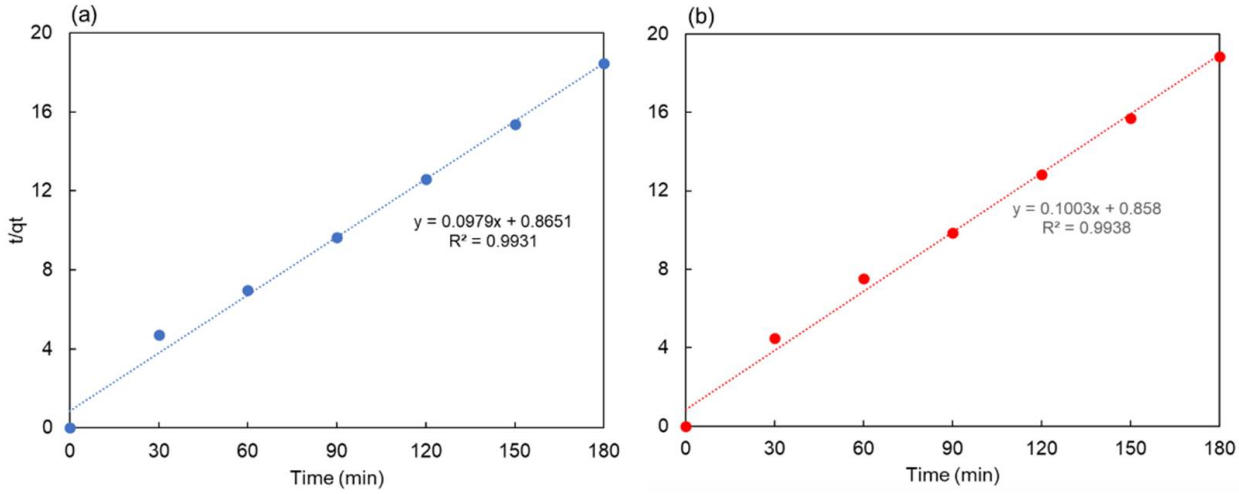

Figure 9. Pseudo second-order kinetics of STOn (**a**) and STOm (**b**).

In more detail, only STOn used in large amount (1.00 g·L^{-1}) permits one to reach 25% DCF mineralization, thanks to its nanometric dimension, which make the oxide particularly active. In all the other cases, the mineralization was poor. These findings are in line with those previously obtained by ZnO and TiO_2 under UV light irradiation [12,18].

Based on all these results, the effect of water matrix was investigated, carrying out the DCF photodegradation by both STOm and STOn (0.25 g·L^{-1}) in DW to evaluate the effect of the presence of inorganic salts on DCF photodegradation (Figure 10).

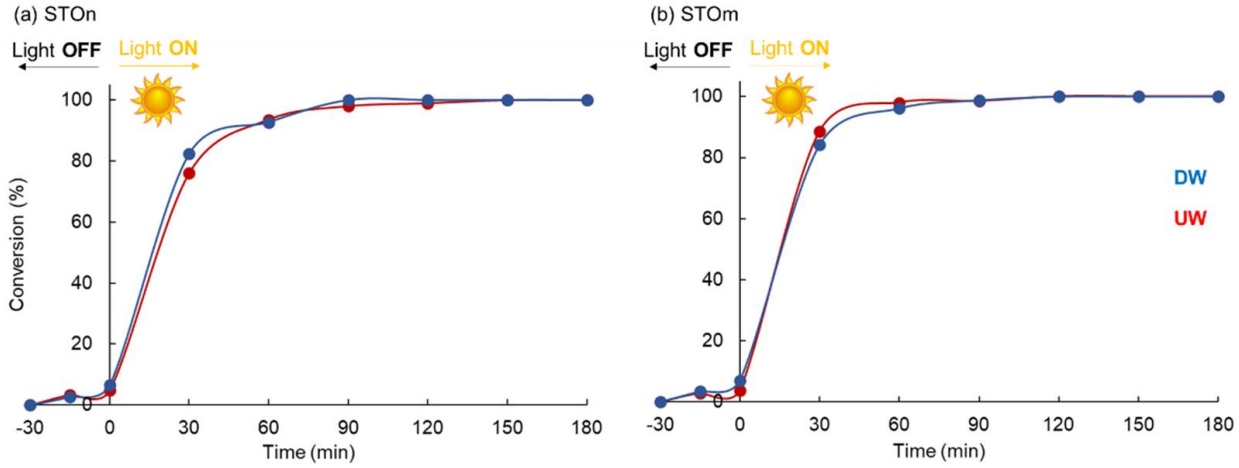

Figure 10. Effect of water matrix on DCF photodegradation by STOn and STOm (UW = ultrapure water; DW = simulated drinking water).

All samples retained their degradation performance in both UW and DW, indicating that electrolytes do not have a detrimental effect on the DCF photodegradation. Previous studies, carried out with other oxides (ZnO and TiO_2), reported different results, demonstrating that TiO_2 worsens its photocatalytic performance in DW [18], whereas on the contrary, ZnO enhances its photocatalytic efficiency [12,18]. These findings are particularly important. In fact, a large number of investigations on DCF photodegradation confirmed the negative effects of electrolytes in different water matrices [75] due to the presence of inorganic species (chlorides, carbonates, bicarbonates, etc.) that can block active sites at the photocatalyst surface, as well as compete for free radicals. In addition, high values of ionic strength can also cause agglomeration phenomena with negative consequences on the available surface area of the photocatalyst. All these aspects do not seem to affect the photocatalytic properties of STO, which maintains the same efficiency regardless of size.

For practical applications, a useful photocatalyst requires stability to be reused many times without losing performance. In addition, it is important to remember that in the last years, great concerns have been risen regarding the effective toxicity of nanomaterials.

Particles with dimensions below 100 nm fall into the class of "ultrafine" materials [76], exhibiting several adverse health effects, such as lung tumors, inflammations, fibrosis, DNA damage, and so on [77,78], owing to their ability to deeply penetrate lungs and cell membranes [77].

Moreover, compared to nanometric materials, micro-sized particles are more easily recoverable by traditional filtration, greatly reducing process costs.

For all these reasons, reusability tests were carried out on STOm (1.00 $g \cdot L^{-1}$) in both UW and DW (Figure 11).

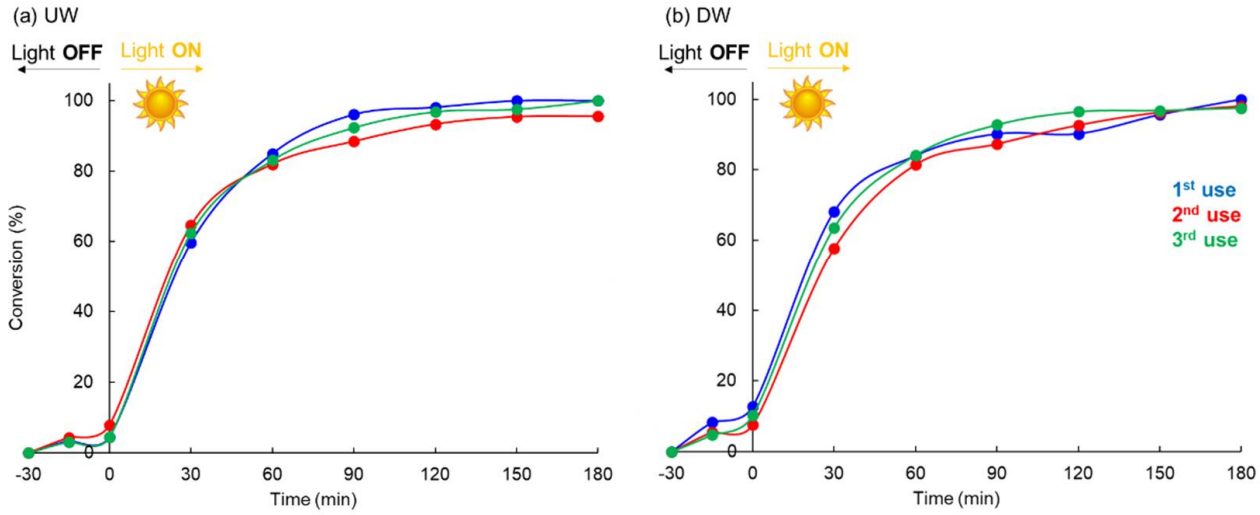

Figure 11. Reusability tests of STOm (1.00 $g \cdot L^{-1}$) towards DCF photodegradation in UW (**a**) and DW (**b**).

As can be observed, a good reproducibility of performances was observed after three-run recycling, guaranteeing a good stability of STOm under the used conditions, as confirmed by XRPD and FT-IR analyses carried out on the used sample (Figure S6).

To understand the degradation pathway of various photocatalysts, active species trapping experiments are particularly useful. A number of photogenerated species, including h^+, OH, and O_2^-, play an important role in the photocatalytic degradation process. To trap h^+, OH, and O_2^- scavengers, such as disodium ethylenediaminetetraacetic acid (Na_2-EDTA), p-benzoquinone (BQ), and isopropyl alcohol (IPA) can be used. The reactive species trapping experiments were carried out during DCF photodegradation in the presence of STOm (1.00 $g \cdot L^{-1}$) as photocatalyst in UW. Results are summarized in Figure 12.

It is possible to observe that the addition of BQ (an O_2 scavenger) greatly diminishes the percentage of DCF that degrades, suggesting that O_2-photogenerated charge carriers are of much importance in this photocatalytic activity. In contrast, the addition of EDTA for trapping h^+ does slightly slow down photocatalytic DCF degradation, indicating that h^+ plays only a minor role in DCF degradation. Eventually, IPA (a OH scavenger) had no effect in photocatalytic DCF degradation.

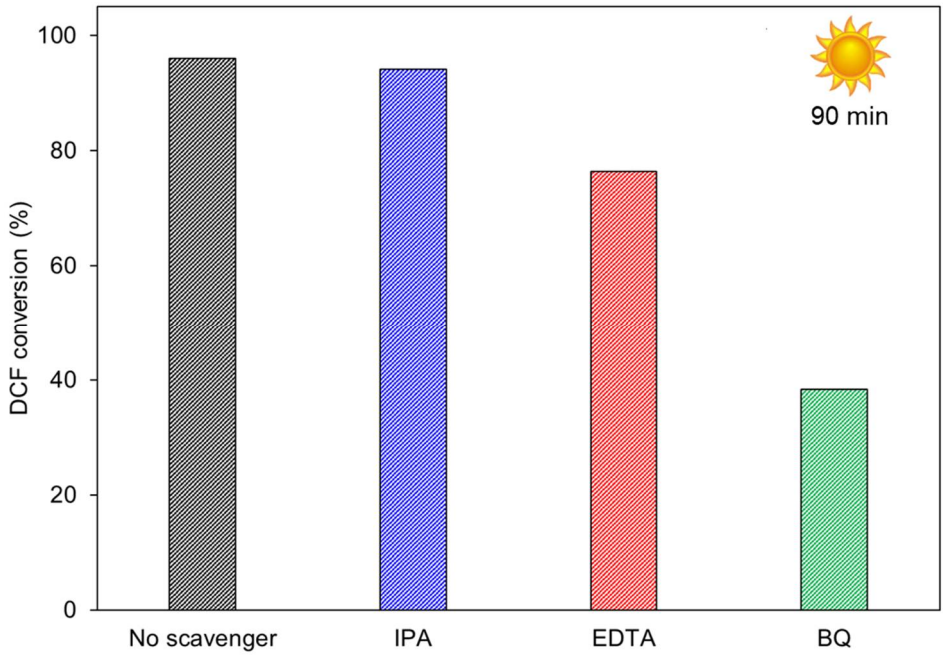

Figure 12. Effect of scavengers (IPA = isopropyl alcohol; EDTA = disodium ethylenediaminetetraacetic acid; BQ = p-benzoquinone) on the photocatalytic degradation of DCF by STOm (1.00 $g \cdot L^{-1}$) in UW.

3. Materials and Methods

3.1. Materials

All chemicals of analytical grade were purchased from Sigma-Aldrich products (Merck & Co, St. Louis, MO, USA). The two purchased catalysts were strontium titanate (99% purity) micro- and nano-powders; they were labelled as STOm and STOn, respectively. Pollutant mixtures were prepared in ultrapure water (UW) and in a simulated solution of drinking water (DW), whose composition is reported below. For HPLC/UV analyses, HPLC-grade acetonitrile and water were purchased from Carlo Erba reagents.

3.2. Characterization

Sample morphology was evaluated by scanning electron microscopy and conventional electron microscopy (SEM and C-TEM, respectively). Concerning the former, images were collected using a Zeiss LEO 1525 field emission microscope (Overcoached, Germany) without any sample pretreatment. Regarding the latter, images were collected by means of a Jeol JEM 3010-UHR instrument (LaB6 filament, acceleration voltage 300 kV, Milpitas, CA, USA), equipped with a Gatan Ultrascan 1000 camera. In this case, for sample preparation, powders were milled in an agate mortar and deposited on a Cu grid covered with a lacey carbon.

Crystal structure and phase composition of samples were determined by X-ray powder diffraction (XRPD) by means of a PANanalytical X'Pert PRO diffractometer (Cu Kα = 1.54060 Å and equipped with X-ray source operating at 40 kV × 40 mA). All the diffractograms were collected in 10–80° (2θ) range, with a step of 0.02° 2θ (or 0.05° 2θ), and the time for each step in the interval of 5–96 s. Before the analyses, powders were finely ground and spread on an aluminum flat-plate horizontal sample holder. Patterns were identified by comparison with the JCPDS files from International Center for Diffraction Data Powder Diffraction. The average crystallite size (D) was evaluated by Scherrer equation (Equation (2)) using the peaks at 46.52° (corresponding to 200 reflection), as follows:

$$D = \frac{K\Delta\lambda}{\beta \cdot cos\theta} \quad (2)$$

where K is the shape factor, λ is the wavelength of X-ray radiation, θ is the diffraction Bragg angle, and β is the corrected peak width at half the maximum.

Specific surface area (SA) and porosity (pore volume, pore size, and pore size distribution) were determined by N_2 adsorption/desorption isotherms collected at −196 °C using an automatic analyzer of surface area (Coulter SA3100 instrument, Beckman Life Sciences, Los Angeles, CA, USA). Before each analysis, ca. 0.50 g dried sample was outgassed at 150 °C for 4 h under vacuum to remove water and other volatile organic compounds adsorbed on the surface. Specific surface area values were calculated by Brunauer–Emmet–Teller (BET) equation (two parameters, $0.05 < p/p_0 < 0.3$), considering a cross-sectional area of ca. 16.2 Å LATIN CAPITAL/molecule$_{N2}$. Pore volume and pore size distribution (PSD) were determined by Barrett–Joyner–Halenda (BJH) model from the desorption branch of the collected isotherms (range: $0.3 < p/p_0 < 0.95$).

Fourier transform infrared (FT-IR) spectra were collected in the 400−4000 cm^{-1} interval at room temperature through a Perkin-Elmer spectrometer (Perkin Elmer, Waltham, MA, USA). Prior to the analysis, samples were dried at 120 °C overnight, and then ca. 5 mg of each dried sample was padded in mixture with ca. 200 mg of dried KBr (sample to KBr weight ratio ca. 1:40).

UV-Vis diffuse reflectance (UV-DR) spectra were collected at room temperature in the 200−800 nm interval through a double-beam UV–Vis–NIR scanning spectrophotometer (Perkin Elmer Lambda 750s UV-Vis spectrophotometer, Perkin Elmer, Waltham, MA, USA) equipped with an integrating sphere assembly. Each sample in powder form was finely ground, uniformly pressed in a circular disk (E.D., ca. 4 cm), and included in the sample-holder. This latter was inserted in a special quartz cuvette and placed on the window of the integrating sphere for reflectance measurements. Spectra were measured using lab sphere reflectance standards consisting of $BaSO_4$ as the reference. The measured reflectance values (R%) were converted to absorbance (Abs, a.u.) by the following equation:

$$\text{Abs} = \text{Log}\,(1/R/100) \quad (3)$$

The isoelectric point (IEP) of samples was determined according to the following procedure, previously reported in the literature [7]. In a typical experiment, ca. 50 mg of sample powder was weighed and introduced in $NaNO_3$ solutions (20 mL, 0.1 M) under stirring. Initial pH values ($pH_{initial}$) of $NaNO_3$ solutions were adjusted in 4.00−10.00 intervals, adding 0.1 M HNO_3 or NaOH. Suspensions were maintained under stirring (250 rpm) for 24 h, and successively, the final pH values (pH_{final}) were measured after suspension centrifuge (3000 rpm for 6 min). By plotting the difference between the pH_{final} and $pH_{initial}$ (ΔpH) along with the $pH_{initial}$, pH_{pzc} was determined as the intersection of the resulting line at which $\Delta pH = 0$.

Surface composition of samples was studied by X-ray photoelectron spectroscopy (XPS) by means of an M-PROBE Surface Spectrometer with an Al (Kα) source and a spot size from 0.15 mm to 1 mm in diameter (USA). A 10 V applied voltage at a vacuum of 10^{-7} –10^{-8} Torr was used. Survey scans were investigated in 0−1100 eV binding energy range, using a spot size of 800 microns with 4 eV energy resolution (scan rate of 1 eV per step). ESCA Hawk Software was used for data curation. Charge neutralization was carried out by means of a low-energy electron beam. In any case, the resulting binding energy values (BE) were corrected by setting the C 1s peak (C–C) fixed at 284.6 eV as the reference. The C 1s photopeak comprised four components (C–C, C–O, and C=O bonds, as well as a specific feature corresponding to CO_3^{2-}) with respective binding energies of 284.6, 285.9, 287.0, and 289.5 eV (Figure S2). Normalized surface concentrations of all the species were computed by ruling out the contribution of adventitious carbon (C–C at 284.6 eV) [66,79].

3.3. Diclofenac Abatement

Photocatalytic activity was studied in the absorption and photodegradation of DCF in ultrapure and simulated drinking water (UW and DW, respectively). The latter was

prepared according to Annex B2 of the second protocol of the French Norm NF P41-650 regarding the specification for water filter pitchers (Table 1) [80].

Table 1. Ionic species and relative concentration for the preparation of DW.

Species	Concentration (ppm)
Ca^{2+}	44.5
Na^{+}	45.7
Mg^{2+}	9.3
Cl^{-}	78.7
$SO_4{}^{2-}$	36.5
$HCO_3{}^{-}$	121.2

Experiments in UW and DW were performed by stirring 0.100, 0.050, and 0.025 g powder catalyst in a 250 mL batch glass reactor filled with 100 mL pollutant solution (10 ppm), maintained at spontaneous pH (about 5 for UW and 8 for DW, respectively).

The suspension was kept in the dark for 30 min, and it was successively irradiated for 180 min with a solar lamp (power density of irradiation of 35 $W \cdot m^{-2}$, ULTRA VITALUX 300W-OSRAM, Osram, Munich, Germany) placed above the reactor. DCF abatement was monitored for 210 min by sampling aliquots every 15 min in the first half-hour and every 30 min in the subsequent 3 h. Suspensions were centrifuged for 10 min at 135 × 1000 rpm, and the liquid part was analyzed with high-performance liquid chromatography (HPLC). Chromatographic analysis was performed with an isocratic elution of a mobile phase, composed by water (50%), acetonitrile (50%), and formic acid (0.1%), at 1.00 $mL \cdot min^{-1}$. The HPLC instrument (Agilent 1100 Series, Agilent, Santa Clara, CA, USA) was equipped with a C18 Supelco column (25 cm × 4 mm, 5 µm), a 20 µL autosampler, and a UV detector. DCF loss was monitored at 276 nm. In addition, the determination of total organic carbon (TOC) of the sampling aliquots at the beginning and at the end of experiments was carried out by means of a total organic carbon analyzer (TOC-L, Shimadzu, Kyoto, Japan).

After the first abatement test, the STO sample showing the best performances was recovered, washed with water, and then used for two further cycles.

Tests in the presence of disodium ethylenediaminetetraacetate (EDTA), benzoquinone (BQ), and isopropyl alcohol (IPA) as scavengers for holes (h^{+}), superoxide radical ($O_2{}^{-}$), and hydroxyl radical (OH), respectively, were carried out. In these cases, the experimental procedures were conducted as previously reported for typical tests but with the addition of 3 mmol of each scavenger.

4. Conclusions

In this work, the potentialities of nano- and micro-sized strontium titanates in the photodegradation of diclofenac were comparatively investigated. Solar light as source, renewable in nature, was used for the photodegradation of diclofenac. Results indicate that both photocatalysts are promising for DCF abatement under solar light irradiation and maintain the same activity in a complex environment (simulated drinking water), indicating that the presence of electrolytes does not hinder $SrTiO_3$ performance. Moreover, it was demonstrated that the photocatalytic degradation of diclofenac is mostly due to $O_2{}^{-}$ radical species, as indicated by radical trapping investigations. After recycling the catalyst three times, it maintains high photocatalytic performance. Based on these results, $SrTiO_3$ could be considered as a promising alternative to traditional materials to remove hazardous compounds from water.

Supplementary Materials: The following supporting information can be downloaded at: https://www.mdpi.com/article/10.3390/catal12080804/s1, Table S1: Surface composition of the studied STO samples determined by XPS obtained by subtraction of adventitious carbon (at 284.6 eV); Figure S1: Survey spectra of STOm and STOn (left and right, respectively); Figure S2: HR C 1s spectrum of STOn; Figure S3: Isoelectric point (IEP) of STOm (red line) and STOn (blue line); Figure S4: Photolysis study for DCF decomposition without any catalyst; Figure S5: Percentage of DCF mineralization by STOm and STOn in UW; Figure S6: FT-IR spectra and XRPD pattern of used STOm.

Author Contributions: Conceptualization, E.F. and C.L.B.; methodology, E.F. and G.C.; software, M.G.G. and A.G.; formal analysis, E.F., M.G.G., A.G. and G.C.; investigation, M.G.G. and A.G.; resources, C.L.B.; data curation, E.F., C.L.B. and A.G.; writing—original draft preparation, E.F. and M.G.G.; writing—review and editing, E.F. and C.L.B.; supervision, C.L.B.; funding acquisition, C.L.B. All authors have read and agreed to the published version of the manuscript.

Funding: Velux Stiftung Foundation is gratefully acknowledged for their financial support through the project 1381 "SUNFLOAT—Water decontamination by sunlight-driven floating photocatalytic systems".

Data Availability Statement: The data that support the plots within this paper are available from the corresponding author on reasonable request.

Conflicts of Interest: The authors declare no conflict of interest.

References

1. Shahid, M.K.; Kashif, A.; Fuwad, A.; Choi, Y. Current advances in treatment technologies for removal of emerging contaminants from water—A critical review. *Coord. Chem. Rev.* **2021**, *442*, 213993. [CrossRef]
2. Sophia, C.A.; Lima, E.C. Removal of emerging contaminants from the environment by adsorption. *Ecotoxicol. Environ. Saf.* **2018**, *150*, 1–17. [CrossRef]
3. Alalm, M.G.; Djellabi, R.; Meroni, D.; Pirola, C.; Bianchi, C.L.; Boffito, D.C. Toward Scaling-Up Photocatalytic Process for Multiphase Environmental Applications. *Catalysts* **2021**, *11*, 562. [CrossRef]
4. Djellabi, R.; Giannantonio, R.; Falletta, E.; Bianchi, C.L. SWOT analysis of photocatalytic materials towards large scale environmental remediation. *Curr. Opin. Chem. Eng.* **2021**, *33*, 100696. [CrossRef]
5. Wang, Q.; Yang, Z. Industrial water pollution, water environment treatment, and health risks in China. *Environ. Pollut.* **2016**, *218*, 358–365. [CrossRef] [PubMed]
6. World Health Organization & United Nations Children's Fund (UNICEF). Progress on Sanitation and Drinking Water—2015 Update and MDG Assessment. 2015. Available online: https://apps.who.int/iris/handle/10665/177752 (accessed on 15 July 2022).
7. Bianchi, C.L.; Djellabi, R.; Della Pina, C.; Falletta, E. Doped-polyaniline based sorbents for the simultaneous removal of heavy metals and dyes from water: Unravelling the role of synthesis method and doping agent. *Chemosphere* **2022**, *286*, 131941. [CrossRef]
8. Taheran, M.; Naghdi, M.; Brar, S.K.; Verma, M.; Surampalli, R.Y. Emerging contaminants: Here today, there tomorrow! *Environ. Nanotechnol. Monit. Manag.* **2018**, *10*, 122–126. [CrossRef]
9. Crini, G.; Lichtfouse, E. Advantages and disadvantages of techniques used for wastewater treatment. *Environ. Chem. Lett.* **2019**, *17*, 145–155. [CrossRef]
10. Sonune, A.; Ghate, R. Developments in wastewater treatment methods. *Desalination* **2004**, *167*, 55–63. [CrossRef]
11. Saber, A.N.; Djellabi, R.; Fellah, I.; Abderrahim, N.; Bianchi, C.L. Synergistic sorption/photo-Fenton removal of typical substituted and parent polycyclic aromatic hydrocarbons from coking wastewater over CuO-Montmorillonite. *J. Water Process Eng.* **2021**, *44*, 102377. [CrossRef]
12. Meroni, D.; Bianchi, C.L.; Boffito, D.C.; Cerrato, G.; Bruni, A.; Sartirana, M.; Falletta, E. Piezo-enhanced photocatalytic diclofenac mineralization over ZnO. *Ultrason. Sonochem.* **2021**, *75*, 105615. [CrossRef] [PubMed]
13. Kanakaraju, D.; Glass, B.D.; Oelgemöller, M. Advanced oxidation process-mediated removal of pharmaceuticals from water: A review. *J. Environ. Manag.* **2018**, *219*, 189–207. [CrossRef]
14. Garrido-Cardenas, J.A.; Esteban-García, B.; Agüera, A.; Sánchez-Pérez, J.A.; Manzano-Agugliaro, F. Wastewater Treatment by Advanced Oxidation Process and Their Worldwide Research Trends. *Int. J. Environ. Res. Public Health* **2019**, *17*, 170. [CrossRef] [PubMed]
15. Cerrato, G.; Bianchi, C.L.; Galli, F.; Pirola, C.; Morandi, S.; Capucci, V. Micro-TiO_2 coated glass surfaces safely abate drugs in surface water. *J. Hazard. Mater.* **2019**, *363*, 328–334. [CrossRef]
16. Stucchi, M.; Cerrato, G.; Bianchi, C.L. Ultrasound to improve both synthesis and pollutants degradation based on metal nanoparticles supported on TiO_2. *Ultrason. Sonochem.* **2019**, *51*, 462–468. [CrossRef]
17. Schieppati, D.; Galli, F.; Peyot, M.-L.; Yargeau, V.; Bianchi, C.L.; Boffito, D.C. An ultrasound-assisted photocatalytic treatment to remove an herbicidal pollutant from wastewaters. *Ultrason. Sonochem.* **2019**, *54*, 302–310. [CrossRef]

18. Meroni, D.; Jiménez-Salcedo, M.; Falletta, E.; Bresolin, B.M.; Kait, C.F.; Boffito, D.C.; Bianchi, C.; Pirola, C. Sonophotocatalytic degradation of sodium diclofenac using low power ultrasound and micro sized TiO_2. *Ultrason. Sonochem.* **2020**, *67*, 105123. [CrossRef]
19. Kavitha, S.; Ranjith, R.; Jayamani, N.; Vignesh, S.; Palanivel, B.; Djellabi, R.; Bianchi, C.L.; Alharthi, F.A. Fabrication of visible-light-responsive TiO_2/α-Fe_2O_3-heterostructured composite for rapid photo-oxidation of organic pollutants in water. *J. Mater. Sci. Mater. Electron.* **2022**, *33*, 8906–8919. [CrossRef]
20. Monllor-Satoca, D.; Bonete, P.; Djellabi, R.; Cerrato, G.; Operti, L.; Gomez, R.; Bianchi, C.L. Comparative Photo-Electrochemical and Photocatalytic Studies with Nanosized TiO_2 Photocatalysts towards Organic Pollutants Oxidation. *Catalysts* **2021**, *11*, 349. [CrossRef]
21. Nasr, M.; Eid, C.; Habchi, R.; Miele, P.; Bechelany, M. Recent Progress on Titanium Dioxide Nanomaterials for Photocatalytic Applications. *ChemSusChem* **2018**, *11*, 3023–3047. [CrossRef]
22. Gopinath, K.P.; Madhav, N.V.; Krishnan, A.; Malolan, R.; Rangarajan, G. Present applications of titanium dioxide for the photocatalytic removal of pollutants from water: A review. *J. Environ. Manag.* **2020**, *270*, 110906. [CrossRef] [PubMed]
23. Basavarajappa, P.S.; Patil, S.B.; Ganganagappa, N.; Reddy, K.R.; Raghu, A.V.; Reddy, C.V. Recent progress in metal-doped TiO_2, non-metal doped/codoped TiO_2 and TiO_2 nanostructured hybrids for enhanced photocatalysis. *Int. J. Hydrog. Energy* **2020**, *45*, 7764–7778. [CrossRef]
24. Nasirian, M.; Lin, Y.P.; Bustillo-Lecompte, C.F.; Mehrvar, M. Enhancement of photocatalytic activity of titanium dioxide using non-metal doping methods under visible light: A review. *Int. J. Environ. Sci. Technol.* **2018**, *15*, 2009–2032. [CrossRef]
25. Stucchi, M.; Bianchi, C.L.; Argirusis, C.; Pifferi, V.; Neppolian, B.; Cerrato, G.; Boffito, D.C. Ultrasound assisted synthesis of Ag-decorated TiO_2 active in visible light. *Ultrason. Sonochem.* **2018**, *40*, 282–288. [CrossRef]
26. Stucchi, M.; Boffito, D.C.; Pargoletti, E.; Cerrato, G.; Bianchi, C.L.; Cappelletti, G. Nano-MnO_2 Decoration of TiO_2 Microparticles to Promote Gaseous Ethanol Visible Photoremoval. *Nanomaterials* **2018**, *8*, 686. [CrossRef]
27. Falletta, E.; Bruni, A.; Sartirana, M.; Boffito, D.C.; Cerrato, G.; Giordana, A.; Djellabi, R.; Khatibi, E.S.; Bianchi, C.L. Solar Light Photoactive Floating Polyaniline/TiO_2 Composites for Water Remediation. *Nanomaterials* **2021**, *11*, 3071. [CrossRef]
28. Serga, V.; Burve, R.; Krumina, A.; Pankratova, V.; Popov, A.I. Study of phase composition, photocatalytic activity, and photoluminescence of TiO_2 with Eu additive produced by the extraction-pyrolytic method. *J. Mater. Res. Technol.* **2021**, *13*, 2350–2360. [CrossRef]
29. Mergenbayeva, S.; Kumarov, A.; Atabaev, T.S.; Hapeshi, E.; Vakros, J.; Mantzavinos, D.; Poulopoulos, S.G. Degradation of 4-Tert-Butylphenol in Water Using Mono-Doped (M1: Mo, W) and Co-Doped (M2-M1: Cu, Co, Zn) Titania Catalysts. *Nanomaterials* **2022**, *12*, 2326. [CrossRef]
30. Wu, X.; Lin, J.; Xu, Z.; Zhao, C.; Lin, C.; Wang, H.; Lin, T.; Zheng, X.; Sa, B.; Zhang, Q.; et al. Defect Management and Multi-Mode Optoelectronic Manipulations via Photo-Thermochromism in Smart Windows. *Laser Photonics Rev.* **2021**, *15*, 2100211. [CrossRef]
31. Shi, L.; Chen, K.; Zhai, A.; Li, G.; Fan, M.; Hao, Y.; Zhu, F.; Zhang, H.; Cui, Y. Status and Outlook of Metal–Inorganic Semiconductor–Metal Photodetectors. *Laser Photonics Rev.* **2020**, *15*, 2000401. [CrossRef]
32. Yang, B.; Wang, M.; Hu, X.; Zhou, T.; Zang, Z. Highly efficient semitransparent CsPbIBr2 perovskite solar cells via low-temperature processed In2S3 as electron-transport-layer. *Nano Energy* **2019**, *57*, 718–727. [CrossRef]
33. da Silva, L.F.; Lopes, O.F.; de Mendonça, V.R.; Clavalho, K.T.G.; Longo, E.; Ribeiro, C.; Mastelaro, V.R. An understanding of the photocatalytic properties and pollutant degradation mechanism of $SrTiO_3$ nanoparticles. *Photochem. Photobiol.* **2016**, *92*, 371–378. [CrossRef]
34. Zhu, J.; Zhu, M.; Shi, Q.; Wen, F.; Liu, L.; Dong, B.; Haroun, A.; Yang, Y.; Vachon, P.; Guo, X.; et al. Progress in TENG technology—A journey from energy harvesting to nanoenergy and nanosystem. *EcoMat* **2020**, *2*, e12058. [CrossRef]
35. Dong, Z.; Chen, H.; Qi, M.; Shen, J.; Liu, W.; Guo, E.-J.; Li, D.; Zhang, Y.; Wu, Z. Enhanced Upconversion Photoluminescence Assisted by Flexoelectric Field in Oxide Nanomembranes. *Laser Photonics Rev.* **2022**, *16*, 2100454. [CrossRef]
36. Eglitis, R.I.; Purans, J.; Popov, A.I.; Jia, R. Systematic trends in $YAlO_3$, $SrTiO_3$, $BaTiO_3$, $BaZrO_3$ and (111) surface ab initio calculations. *Int. J. Mod. Phys. B* **2019**, *33*, 1950390. [CrossRef]
37. Chang, C.-W.; Hu, C. Graphene oxide-derived carbon-doped $SrTiO_3$ for highly efficient photocatalytic degradation of organic pollutants under visible light irradiation. *Chem. Eng. J.* **2020**, *383*, 123116. [CrossRef]
38. Hu, C.; Huang, H.-X.; Lin, Y.-F.; Yoshida, M.; Chen, T.-H. Decoration of $SrTiO_3$ nanofibers by BiOI for photocatalytic methyl orange degradation under visible light irradiation. *J. Taiwan Inst. Chem. Eng.* **2019**, *96*, 264–272. [CrossRef]
39. Kumar, A.; Kumar, A.; Krishnan, V. Perovskite Oxide Based Materials for Energy and Environment-Oriented Photocatalysis. *ACS Catal.* **2020**, *10*, 10253–10315. [CrossRef]
40. Kong, J.; Yang, T.; Rui, Z.; Ji, H. Perovskite-based photocatalysts for organic contaminants removal: Current status and future perspectives. *Catal. Today* **2019**, *327*, 47–63. [CrossRef]
41. Djellabi, R.; Ordonez, M.F.; Conte, F.; Falletta, E.; Bianchi, C.L.; Rossetti, I. A review of advances in multifunctional $XTiO_3$ perovskite-type oxides as piezo-photocatalysts for environmental remediation and energy production. *J. Hazard. Mater.* **2022**, *421*, 126792. [CrossRef]
42. Weldegebrieal, G.K. Synthesis method, antibacterial and photocatalytic activity of ZnO nanoparticles for azo dyes in wastewater treatment: A review. *Inorg. Chem. Commun.* **2020**, *120*, 108140. [CrossRef]

43. Aliste, M.; Garrido, I.; Flores, P.; Hellin, P.; Vela, N.; Navarro, S.; Fenoll, J. Reclamation of agro-wastewater polluted with thirteen pesticides by solar photocatalysis to reuse in irrigation of greenhouse lettuce grown. *J. Environ. Manage.* **2020**, *266*, 110565. [CrossRef] [PubMed]
44. Kushniarou, A.; Garrido, I.; Fenoll, J.; Vela, N.; Flores, P.; Navarro, G.; Hellin, P.; Navarro, S. Solar photocatalytic reclamation of agro-waste water polluted with twelve pesticides for agricultural reuse. *Chemosphere* **2019**, *214*, 839–845. [CrossRef] [PubMed]
45. Arnab, D.; Rituparna, B.; Ajeet, K.; Subho, M. *Targeted Delivery of Pesticides Using Biodegradable Polymeric Nanoparticles*; Springer: New Delhi, India, 2014.
46. UNEP. *The Snapshot Report of the World's Water Quality*; UNEP: Nairobi, Kenya, 2016.
47. Iovino, P.; Chianese, S.; Canzano, S.; Pisciandaro, M.; Musmarra, D. Photodegradation of diclofenac in wastewaters. *Desalin. Water Treatment* **2017**, *61*, 293–297.
48. Calza, P.; Sakkas, V.A.; Villioti, A.; Massolino, C.; Boti, V.; Pelizzetti, E.; Albanis, T. Multivariate experimental design for the photocatalytic degradation of imipramine, determination of the reaction pathway and identification of intermediate products. *Appl. Catal. B Environ.* **2008**, *84*, 379–388. [CrossRef]
49. Wiegel, S.; Aulinger, A.; Brockmeyer, R.; Harms, H.; Löffler, J.; Reincke, H. Pharmaceuticals in the river Elbe and its tributaries. *Chemosphere* **2004**, *57*, 107–126. [CrossRef]
50. Fent, K.; Weston, A.; Caminada, D. Ecotoxicology of human pharmaceuticals. *Aquat. Toxicol.* **2006**, *76*, 122–159. [CrossRef]
51. Radjenovic, J.; Petrovic, M.; Barceló, D. Analysis of pharmaceuticals in wastewater and removal using a membrane bioreactor. *Anal. Bioanal. Chem.* **2007**, *387*, 1365–1377. [CrossRef]
52. Vieno, N.M.; Harkki, H.; Tuhkanen, T.; Kronberg, L. Occurrence of pharmaceuticalsin river water and their elimination in a pilot-scale drinking water treatment plant. *Environ. Sci. Technol.* **2007**, *41*, 5077–5084. [CrossRef]
53. Hartmann, J.; Bartels, P.; Mau, U.; Witter, M. Degradation of the drug diclofenac in water by sonolysis in presence of catalysts. *Chemosphere* **2008**, *70*, 453–461. [CrossRef]
54. Ahmed, M.A.; Abou-Gamra, Z.M.; Medien, H.A.A.; Hamza, M.A. Effect of porphyrin on photocatalytic activity of TiO_2 nanoparticles toward Rhodamine B photodegradation. *J. Photochem. Photobiol. B Biol.* **2017**, *176*, 25–35. [CrossRef] [PubMed]
55. Quesada, H.B.; Baptista, A.T.A.; Cusioli, L.F.; Seibert, D.; de Oliveira Bezerra, C.; Bergamasco, R. Surface water pollution by pharmaceuticals and an alternative of removal by low-cost adsorbents: A review. *Chemosphere* **2019**, *222*, 766–780. [CrossRef] [PubMed]
56. European Union. Directive 2013/39/EU of the european parliament and of the council. *Off. J. Eur. Union* **2013**, *226*, 1–17.
57. Rodrigues, A.S.; Silveira, J.E.; Carbajo, J.; Zazo, J.A.; Casas, J.A.; Fernandes, A.; Pacheco, M.J.; Ciriaco, L.; Lopes, A. Diclofenac photodegradation with the Perovskites $BaFe_yTi_{1-y}O_3$ as catalysts. *Environ. Sci. Pollut. Res.* **2021**, *28*, 23822–23832. [CrossRef] [PubMed]
58. Sabzehmeidani, M.M.; Karimi, H.; Ghaedi, M. Electrospinning preparation of NiO/ZnO composite nanofibers for photodegradation of binary mixture of rhodamine B and methylene blue in aqueous solution: Central composite optimization. *Appl. Organomet. Chem.* **2018**, *32*, e4335. [CrossRef]
59. Gunture; Singh, A.; Bhati, A.; Khare, P.; Tripathi, K.M.; Sonkar, S.K. Soluble Graphene Nanosheets for the Sunlight-Induced Photodegradation of the Mixture of Dyes and its Environmental Assessment. *Sci. Rep.* **2019**, *9*, 2522. [CrossRef]
60. International Organization for Standardization. Determination of the Specific Surface Area of Solids by Gas Adsorption—BET Method. ISO 9277:2. Available online: www.iso.org (accessed on 10 July 2022).
61. Thommes, M.; Kaneko, K.; Neimark, A.V.; Olivier, J.P.; Rodriguez-Reinoso, F.; Rouquerol, J.; Sing, K.S.W. Physisorption of gases, with special reference to the evaluation of surface area and pore size distribution (IUPAC Technical Report). *Pure App. Chem.* **2015**, *87*, 1051–1069. [CrossRef]
62. ALOthman, Z.A. A review: Fundamental aspects of silicate mesoporous materials. *Materials* **2012**, *5*, 2874–2902. [CrossRef]
63. Sotomayor, F.J.; Cychosz, K.A.; Thommes, M. Characterization of Micro/Mesoporous Materials by Physisorption: Concepts and Case Studies. *Acc. Mater. Surf. Res.* **2018**, *3*, 34–50.
64. Nagarkar, P.V.; Searson, P.C.; Gealy III, F.D. Effect of surface treatment on $SrTiO_3$: An x-ray photoelectron spectroscopic study. *J. Appl. Phys.* **1991**, *69*, 459. [CrossRef]
65. Shibagaki, S.; Fukushima, K. XPS analysis on Nb–$SrTiO_3$ thin films deposited with pulsed laser ablation technique. *J. Eur. Ceram. Soc.* **1999**, *19*, 1423–1426. [CrossRef]
66. Lefebvre, J.; Galli, F.; Bianchi, C.L.; Patience, G.-S.; Boffito, D.C. Experimental Methods in Chemical Engineering: X-Ray Photoelectron Spectroscopy—XPS. *Can. J. Chem. Eng.* **2019**, *97*, 2588–2593. [CrossRef]
67. Zhou, X.; Liu, N.; Yokosawa, T.; Osvet, A.; Miehlich, M.E.; Meyer, K.; Spiecker, E.; Schmuki, P. Intrinsically Activated $SrTiO_3$: Photocatalytic H_2 Evolution from Neutral Aqueous Methanol Solution in the Absence of Any Noble Metal Cocatalyst. *ACS Appl. Mater. Interfaces* **2018**, *10*, 29532–29542. [CrossRef] [PubMed]
68. Miot, C.; Husson, E.; Proust, C.; Erre, R.; Coutures, J.P. Residual carbon evolution in $BaTiO_3$ ceramics studied by XPS after ion etching. *J. Eur. Ceram. Soc.* **1998**, *18*, 339–343. [CrossRef]
69. Liu, G.; Sun, C.; Yang, H.G.; Smith, S.C.; Wang, L.; Lu, G.Q.; Cheng, H.M. Nanosized anatase TiO_2 single crystals for enhanced photocatalytic activity. *Chem. Commun.* **2010**, *46*, 755–757. [CrossRef]
70. Reinosa, J.J.; Leret, P.; Alvarez-Docio, C.M.; del Campo, A.; Fernandez, J.F. Enhancement of UV absorption behavior inZnO–TiO_2 composites. *Bol. Soc. Esp. Ceram. Vidr.* **2016**, *55*, 55–62. [CrossRef]

71. Zhu, Q.-A.; Xu, J.-G.; Xiang, S.; Chen, L.-X.; Tan, Z.-G. Preparation of $SrTiO_3$ nanoparticles by the combination of solid phase grinding and low temperature calcining. *Mater. Lett.* **2011**, *65*, 873–875. [CrossRef]
72. Jia, A.; Liang, X.; Su, Z.; Zhu, T.; Liu, S. Synthesis and the effect of calcination tempera-ture on the physical-chemical properties and photocatalytic activities of Ni, La codoped $SrTiO_3$. *J. Hazard. Mater.* **2010**, *178*, 233–242. [CrossRef]
73. Yu, P.Y.; Cardona, M. *Fundamentals of Semiconductors: Physics and Materials Properties*, 4th ed.; Springer: Berlin/Heidelberg, Germany, 2010.
74. Chong, M.N.; Jin, B.; Chow, C.W.K.; Saint, C. Recent developments in photocatalytic water treatment technology: A review. *Water Res.* **2010**, *44*, 2997–3027. [CrossRef]
75. Achilleos, A.; Hapeshi, E.; Xekoukoulotakis, N.P.; Mantzavinos, D.; Fatta-Kassinos, D. Factors affecting diclofenac decomposition in water by UV-A/TiO_2 photocatalysis. *Chem. Eng. J.* **2010**, *161*, 53–59. [CrossRef]
76. Hou, J.; Wang, L.; Wang, C.; Zhang, S.; Liu, H.; Li, S.; Wang, X. Toxicity and mechanisms of action of titanium dioxide nanoparticles in living organisms. *J. Environ. Sci.* **2019**, *75*, 40–53. [CrossRef] [PubMed]
77. Park, S.; Lee, S.; Kim, B.; Lee, S.; Lee, J.; Sim, S.; Gu, M.; Yi, J.; Lee, J. Toxic effects of titanium dioxide nanoparticles on microbial activity and metabolic flux. *Biotechnol. Bioprocess Eng.* **2012**, *17*, 276–282. [CrossRef]
78. Oravisjärvi, K.; Pietikäinen, M.; Ruuskanen, J.; Rautio, A.; Voutilainen, A.; Keiski, R.L. Effects of physical activity on the deposition of traffic-related particles into the human lungs in silico. *Sci. Total Environ.* **2011**, *409*, 4511–4518. [CrossRef]
79. Stucchi, M.; Alijani, S.; Manzoli, M.; Villa, A.; Lahti, R.; Galloni, M.G.; Lassi, U.; Prati, L. A Pt-Mo hybrid catalyst for furfural transformation. *Catal. Today* **2020**, *327*, 122–131. [CrossRef]
80. Rimoldi, L.; Meroni, D.; Falletta, E.; Pifferi, V.; Falciola, L.; Cappelletti, G.; Ardizzone, S. Emerging pollutant mixture mineralization by TiO_2 photocatalysts. The role of the water medium. *Photochem. Photobiol. Sci.* **2017**, *16*, 60–66. [CrossRef] [PubMed]